Journal of
Materials Chemistry B

Accepted Manuscript

This article can be cited before page numbers have been issued, to do this please use: P. Kannan, M. Thandavarayan, S. Nanda Gopal and M. Opallo, *J. Mater. Chem. B*, 2013, DOI: 10.1039/C3TB20923G.

This is an *Accepted Manuscript*, which has been through the RSC Publishing peer review process and has been accepted for publication.

Accepted Manuscripts are published online shortly after acceptance, which is prior to technical editing, formatting and proof reading. This free service from RSC Publishing allows authors to make their results available to the community, in citable form, before publication of the edited article. This *Accepted Manuscript* will be replaced by the edited and formatted *Advance Article* as soon as this is available.

To cite this manuscript please use its permanent Digital Object Identifier (DOI®), which is identical for all formats of publication.

More information about *Accepted Manuscripts* can be found in the **Information for Authors**.

Please note that technical editing may introduce minor changes to the text and/or graphics contained in the manuscript submitted by the author(s) which may alter content, and that the standard **Terms & Conditions** and the **ethical guidelines** that apply to the journal are still applicable. In no event shall the RSC be held responsible for any errors or omissions in these *Accepted Manuscript* manuscripts or any consequences arising from the use of any information contained in them.

View Article Online
DOI: 10.1039/C3TB20923G

Nitrogen doped graphene nanosheets supported platinum nanoparticles as high performance electrochemical homocysteine biosensor

Palanisamy Kannan,*[a] Thandavarayan Maiyalagan,*[b] Nanda Gopal Sahoo,[c] and Marcin Opallo [a]

[a] Institute of Physical Chemistry, Polish Academy of Sciences
44/52 ul. Kasprzaka, 01-224 Warszawa, Poland.

[b] Materials Science and Engineering Program
204 E. Dean Keeton St, Stop C2200
The University of Texas at Austin, Austin, TX78712, USA.

[c] Institute of Materials Research and Engineering
3 Research link, Singapore 117602.

*Corresponding author: maiyalagan@gmail.com (Maiyalagan); ktpkannan@gmail.com (Kannan); Phone: +48 223 433 375; Fax: +48 223 433 333.

View Article Online
DOI: 10.1039/C3TB20923G

Abstract

Functional carbon nanomaterials are significantly important for the development of high performance sensitive and selective electrochemical biosensors. In this study, graphene supported platinum nanoparticles (GNs/PtNPs) and nitrogen doped graphene supported platinum nanoparticles (N-GNs/PtNPs) were synthesized by a simple chemical reduction method and explored as high performance nanocatalysts supports as well as doped nanocatalyst supports, toward electrochemical oxidation of homocysteine (HCY) for the first the time. Our studies demonstrate that, N-doped graphene supported PtNPs showing higher electrocatalytic activity of HCY with an experimental detection limit of 200 pM. Moreover, N-doped graphene supported Pt demonstrated as an excellent selectivity in the electrochemical oxidation of HCY i.e., the detection of HCY is successful in the presence of 20-fold excess of ascorbic acid (AA). The practical application of N-doped graphene supported PtNPs material is effectively used for the determination of HCY in both human blood serum and urine samples by differential pulse voltammetry under optimized conditions. Our findings conclude that N-doped graphene supported PtNPs can be developed as an high performance and versatile nano-electrocatalyst for electrochemical biosensor applications.

Keywords: Nitrogen doped graphene nanosheets, Pt nanoparticles, Electrochemical biosensor, Homocysteine.

View Article Online
DOI: 10.1039/C3TB20923G

1. Introduction

Graphene nanosheets (GNs), emerging as an amazing two-dimensional material have shown their fascinating applications in catalysis, bioelectronics, and biosensing.[1-6] Due to its unique physical and chemical properties of graphene, such as higher surface area, tremendous conductivity, easy functionalization and fabrication, provides an ideal support for electric and electronic devices, and biosensors.[7-9] Moreover, developing the electronic characteristics of graphene to achieve unique properties has attracted great attention recently.[10-12] Though, most of these approaches have been aimed to producing graphene hybrids with synergy or multiple functionalities. A little attention has been paid to the intrinsic modification of graphene for the purpose of enhancing the graphene performance in bio-electrochemical systems.[13]

Chemical doping carbon materials with hetero-atoms can effectively tune their intrinsic properties including electronic characteristics, surface structures and local chemical changes to the elemental composition of host materials.[14] It has been also known that, chemical doping is a leading potential strategy to enrich free charge-carrier densities and enhance the thermal or electrical conductivities.[15-17] For instance, graphene is simultaneously etched and its surface doped with oxidation by oxygen etching process.[18] The theoretical investigation of metal doped graphene has been predicted the possibility of a Fermi level shift and a crossover from p-type to n-type.[19] Among the numerous potential dopants, nitrogen is considered to be an excellent element for chemical doping of carbon materials, because it is of comparable atomic size and contains five valence electrons available to form strong valence bonds with carbon atoms, and it has been widely used in the doping of carbon materials.[20, 21] Recent reports have been demonstrated that the nitrogen doping can significantly increasing the electron activity, electron–donor properties and simultaneously enhance their binding ability with guest molecules or materials, which may lead to new properties in device applications.[21-23]

View Article Online
DOI: 10.1039/C3TB20923G

It has been reported that, GNs has a relatively low-density of edge sites relative to its abundant basal plane sites.[24, 25] The GNs tend to stack together because of the strong inter-sheet van der Waals interactions. The stacking of GNs would reduce their porosity, increase the diffusion resistance of reactants/electrolytes, and reduce the number of exposed active sites. Therefore, a careful molecular design of GNs is needed to enable its use as high performance electrochemical biosensors and practical applications. Recently, nitrogen-doped graphene nanosheets (N-GNs) have been explored through chemical vapour deposition, and high temperature annealing methods.[14, 26, 27] Compared to graphene nanosheets (GNs), N-GNs have a large surface-active groups to volume ratio, excellent thermal stability and good electrical and mechanical properties.[28] Recent studies suggested that this kind of material has shown a high efficiency for lithium ion batteries and super-capacitors, and also has effective electrocatalytic activity for the oxygen reduction reaction.[29-31] On the other hand, nanomaterials composed of mono- and bi-metals including Au, Ag, Pt and Pd have also mainly directed the application in electrocatalysis.[32] However, Lee and Wang co-workers have shown that PtNPs-graphene nanocomposites as an excellent materials for electrochemical bio-sensing of glucose and hydrogen peroxide.[33, 34] Ramaprabhu and co-workers successfully used the nitrogen doped Pd nanoparticles decorated graphene nanomaterial for renewable energy related application.[35, 36]

In this paper, we report a strategy to synthesize nitrogen doped graphene supported platinum (N-GN/PtNPs) and graphene supported platinum (GNs-PtNPs) through a simple treatment of graphene by ethylene glycol reduction and further explored the above functionalized graphene as efficient nanomaterial for biosensing of homocysteine (HCY). We discussed a simple approach for biosensing surface modification for selective determination of HCY in the presence of AA and other important interfering molecules. Interestingly, the oxidation potential of HCY at N-GN-PtNPs electrode shifted 210 mV less positively along

View Article Online
DOI: 10.1039/C3TB20923G

with double times of current density enhancement compared to the GNs/PtNPs electrode. The electrical communication between the platinum nanoparticles embedded in the nitrogen doped GNs improved the electrocatalytic properties of the modified electrode toward HCY detection. The N-GN-PtNPs electrode showed excellent sensitivity for HCY detection with the experimental detection limit of 200 pM. The present N-GN-PtNPs electrode is very simple to fabricate and is stable, sensitive, and reproducible. We further demonstrated the determination of HCY in real samples such as human blood plasma and urine using N-doped graphene supported PtNPs modified electrode.

2. Experimental section

2.1. Synthesis of graphene nanosheets (GNs): Graphene oxide sheets were synthesized from expandible graphite flakes by a modified Hummers method.[37] Briefly, expandible graphite (2.0 g) was combined with 50 mL concentrated sulfuric acid in a 250 mL beaker under vigorous agitation at room temperature. Afterwards, sodium nitrate (2.0 g) and potassium permanganate (6.0 g) were slowly poured into the beaker in a sequence. The above mixture was heated at 35ºC for 24 h and then 80 mL of distilled water was added into the solution. 5 min later, 20 mL of 30% H_2O_2 was dropped into the reaction system. Finally, the product was washed with HCl solution and then washed three times with water. The resulting solid was dispersed in water by ultrasonication to make a GNs aqueous dispersion with the concentration of about 4 mg mL.

2.2. Preparation of the nitrogen-doped graphene nanosheets (N-GNs). The graphene nanosheets with high nitrogen content were synthesized through a one-pot process using urea as the chemical dopant.[38] Typically, 10 mL graphene nanosheets (~50 mg) aqueous dispersion was diluted with 25 mL of deionized water, and then a given amount of urea was added into the graphene nanosheets dispersion under sonication for 3 h. After that,

View Article Online
DOI: 10.1039/C3TB20923G

the solution was sealed in a 50 mL Teflon-lined autoclave and maintained at 160 ºC for 6 h. The solids (N-doped graphene nanosheets) were filtered and washed with distilled water several times. Finally, the collected sample was drying in a vacuum oven at 60 ºC and this sample denoted as nitrogen doped graphene. The above procedure is simple and versatile than the nitrogen doped graphene prepared from plasma treatment process.[39]

2.3. Preparation of nitrogen-doped graphene nanosheets supported PtNPs nanocomposite (N-GNs/PtNPs). Several reports in the literature discussed about deposition of Pt nanoparticles (PtNPs).[40-42] In this work, the functionalization of PtNPs on the nitrogen graphene nanosheets was carried out by a chemical co-reduction of Pt precursor salts along with GNs in ethylene glycol (EG)–water solutions.[43, 44] In brief, 100 mg nitrogen doped GNs was added into 100 mL aqueous solution containing 0.02 mM H_2PtCl_6, and then the mixture was ultrasonically treated for 1.5 h to form a stable colloid. Sequentially, 40 mL of EG was injected into the mixture with magnetic stirring for 1 h and then the mixture was kept at 120 ºC for 6 h under magnetic stirring. The final N-GNs/PtNPs composite was collected by filtration, washed with deionized water, and dried in a vacuum desiccator. Our synthetic approach is simpler than the recently Xiong et.al., reported nitrogen doped into the graphene supported Pt nanoparticles.[45] Graphene nanosheets supported PtNPs (GNs/PtNPs) were prepared by using the same procedure for the comparison purpose.

2.4. Characterization methods. The microstructure and morphology of the products were investigated by field emission scanning electron microscopy (FESEM, JEOL JSM 6301F) with an acceleration voltage of 5 kV, and high resolution transmission electron microscopy (TEM, JEOL JEM-2010) with an acceleration voltage of 200 kV measurements, respectively. X-ray diffraction (XRD) patterns were obtained on a Rigaku D/max-IIIB diffractometer using Cu-Kα (l = 1.5406Å) at step scan 0.02θ, from 5 to 80θ. The accelerating

View Article Online
DOI: 10.1039/C3TB20923G

voltage and the applied current were 40 kV and 20 mA. X-ray photoelectron spectroscopy (XPS) analysis was performed on a VG ESCALAB MK II with an MgKα (1253.6 eV) achromatic X-ray source. Electrochemical measurements were performed in a conventional two compartment three electrode cell with a mirror polished 3 mm glassy carbon (GC) as the working electrode, Pt wire as the counter electrode and a NaCl saturated Ag/AgCl as the reference electrode. The electrochemical measurements were carried out with a CHI Model 660C (Austin, TX, USA) electrochemical workstation. In cyclic voltammetry, the electrochemical oxidations of AA and HCY were carried out at a scan rate 50 mV s^{-1}. Pulse width = 0.05 s, amplitude = 0.05 V, sample period = 0.02 s and pulse period = 0.20 s were used in differential pulse voltammetry (DPV). For chronoamperometric measurements, sample interval = 0.1 s and potential step = 0.60 mV were used. All the electrochemical measurements were carried out under a nitrogen atmosphere at room temperature (~27 ºC).

3. Results and discussion

3.1. Morphological characterization of GNs/PtNPs and N-GNs/PtNPs nanocomposites. To control the size and dispersion of Pt nanoparticles on graphene is very important for their application in fuel cells and biosensors.[46, 47] In our studies, we prepared the PtNPs with uniform size and good distribution on graphene nanosheets by controlling the chemical reduction pathway in an aqueous solution. The surface morphology of the nanocomposite was examined by TEM and FE-SEM, XPS and XRD measurements. It can be seen that, Pt/GNs were transparent with voile-like structure corresponding to the planar graphene nanosheets. (Fig. 1A). Further, the FE-SEM image of GNs/PtNPs (Fig. 1A) shows that Pt nanoparticles were spherically shaped, highly dispersed and uniformly distributed on GNs. The low magnification TEM image of GNs/PtNPs (Fig. 1B) shows that Pt nanoparticles were uniformly dispersed over graphene nanosheets with good dispersion. The Pt

View Article Online
DOI: 10.1039/C3TB20923G

nanoparticles were appeared as dots on the graphene nanosheets (bright and dark dots in FE-SEM and TEM images respectively). The distance between the particles was uniform, and the existence of close-packed nanoelectrodes was clearly observed in the TEM image, and now it can be ascribed to the surface functional groups of GNs. We considered 300 nanoparticles for determined by measuring the size of isolated particles, it has been found that the spherical Pt nanoparticles have a narrow size dispersion 8±0.5 nm. It has also been know that, the surface functional groups such as carboxyl, hydroxyl and carbonyl serve as anchoring sites for the metal nanoparticles. Moreover, the oxygen functionalities especially the carboxylic acid can provide an active sites for the nucleation and growth of metal nanoparticles.[48, 49] On the other hand, FE-SEM and TEM images of N-GNs/PtNPs (Fig. 1C, D) consist of randomly crumpled sheets closely associated with each other and forming a disordered solid, which might be attributed to the defective structure formed upon exfoliation and the presence of foreign nitrogen atoms (arrow marks). The GNs morphology were well maintained and clearly observed in TEM image after nitrogen doping, indicating that the features of high surface/volume ratio and the two-dimensional structure of GNs. It is clearly evidenced that nanoparticles on the surface of GNs do not undergo aggregation during nitrogen doping process. The content of Pt nanoparticles into the nitrogen doped GNs hybrid material was measured by ICP (SPS7700, Seiko) instruments and ion loading was calculated as 0.063 mg cm^{-2}. It has been known that, structure of N-Pt/GNs nanocomposite is a sandwich nanostructure, the Pt nanoparticles not only loading on the surface but also in interlayer, so the statistics of the size distribution of wholeness Pt nanoparticles could not be calculated. On the surface of N-GNs/PtNPs, the Pt nanoparticles existed same size distribution (8±0.5 nm diameter) with the coverage of 92.5%. The prepared N-GNs/PtNPs sheets have a thickness of about ~1.8 nm with the lateral size ranging from nanometers to several hundred micrometers.

View Article Online
DOI: 10.1039/C3TB20923G

A pictorial representation showing the possible N locations in the N-GNs/PtNPs nanocomposites (Scheme 1).

3.2. Structural characterization of N-GNs/PtNPs nanocomposites. X-ray photoelectron spectroscopy (XPS) is a powerful tool to identify the elements' states in bulk material.[50] By the analysis of binding energy (BE) values, we have confirmed the nature of nitrogen doping in GNs/PtNPs nanosheets. Core-level high-resolution XPS spectra in the Pt(4f), N1s and C1s binding energies were obtained on N-doped GNs/PtNPs nanosheets. Fig. 2 (a) presents the XPS signature of Pt (4f) doublet ($4f_{7/2}$ and $4f_{5/2}$) deconvoluted into a pair of peaks with binding energies at 71.55 and 74.20 eV for Pt $4f_{7/2}$ and $4f_{5/2}$ were observed, which corresponding to the reduced Pt(0) nanoparticles ensemble. Considering the electrostatic balance, the presence of positively charged Pt ions suggests that there should be a dynamic electron transfer from the Pt nanoparticles to the underlying GNs in the GNs/PtNPs nanohybrids, leading to net negative charges of the GNs. Such an electron transfer from the nanoparticles to graphene is recently confirmed by both theoretical calculation and experimental observation.[51] Furthermore, there is a 0.4 eV positive shift of XPS peak of Pt(0) nanoparticles (71.5 eV) compared with bulk Pt (71.1 eV).[52-55] This shift in the binding energy is typical for very small metal NPs on a variety of support materials, and is generally attributed to reduced core-hole screening in metal nanoparticles/clusters. This result highlights that the electronic properties of the Pt nanoparticles ensemble is significantly different from bulk materials and bigger PtNPs,[52] and such size-dependent alteration of electronic structures likely leads to the unusual electrocatalytic properties. Fig. 2(b) depicts the core level XPS spectra of C1s, which shows the main peak at 284.4 eV corresponds to sp^2 C1s. The small peaks observed at 285.5 eV and 287.1 eV, which are corresponding to the formation of N-sp^2 C and N-sp^3 C bonds, respectively and this would originating from the

View Article Online
DOI: 10.1039/C3TB20923G

substitution of N atom, defects or the edge of the graphene sheets.[56-59] It has been reported that the pristine graphene, the N 1s peak is absent, while in the N-doped graphene, N 1s peak was observed in three components (Fig.2c), indicating that N atoms were in three different bonding characters inserted into the graphene nanosheets. The two peaks observed at 398.37, 400.76 eV correspond to the "pyridinic" and "pyrrolic" N-atom, respectively, they refer to the N atoms which were located in a π conjugated system and contribute to the π system with one or two p-electrons, respectively.[56, 60, 61] Moreover, it has been reported that the pyridinic-N, the nitrogen atom contributes one p-electron to the aromatic p-system and has a lone electron pair in the plane of the ring; as for pyrrolic-N, the nitrogen atom contributes two p-electrons to the p-system, and a hydrogen atom is bound in the plane of the ring, to supporting the graphene skeleton nanosheets.[56, 62] Furthermore, a peak at 401.58 eV corresponds to "graphitic" N, which refers to the N atoms replacing the C atoms inside of the graphene layers.[61] Among the nitrogen doping phases (N1, N2 and N3), nitrogen was dominantly doped in graphene in the form of pyrrolic-N, which preferred to be doped at the edge of graphene in the presence of metal nanoparticles.[35] The nitrogen content within the sample has been calculated from the XPS results and it was approximately 9.5 at.%. In addition, from the XPS analysis it was observed that the contents of pyridinic and graphitic nitrogen atoms are more within the GNs/PtNPs nanosheets.

3.3. X-ray diffraction analysis of N-GNs/PtNPs nanocomposites. Fig. 3 shows the XRD pattern of N-GNs/PtNPs and GNs/PtNPs nanocomposites. The reduced graphene (GNs) showed a broad diffraction peak observed at 27.2º in Fig. 2 (Inset) corresponds to the (002) plane of graphitic carbon, indicates that the presence of reduced graphene in the as prepared nanocomposites. This broadening of the diffraction peak suggests the lack of long-range ordered signature of graphene-based nanocomposites. The largely reduced (002) interlayer

View Article Online
DOI: 10.1039/C3TB20923G

spacing of 0.35 nm in comparison with 0.79 nm of the graphene oxide (GO) revealed that most of the oxygen functional groups intercalated into the interlayer spacing of graphite had been removed during this reduction process. It has been know that GO showed a sharp diffraction peak at 2θ=11.2º, suggesting the complete exfoliation of graphite.[63] Diminution in the interplanar spacing of reduced GO as compared to GO is due to removal of the intercalated water molecules and the oxide groups that allow graphene nanosheets to be tightly packed.[64] A relatively lower intensity peak that occurs at 43º (2.09 Aº) corresponds to (001) plane of reduced GO.[65] The number of layers (four) of the RGO has been obtained using the Debye–Scherrer equation.[65-67]

$$t = 0.9\lambda/\beta_{002}\cos\theta_{002} \qquad \text{(i)}$$

$$n = t/d_{002} \qquad \text{(ii)}$$

where t is thickness; β_{002} is full width at half maximum (FWHM) corresponding to (002) plane; n is the number of graphene layers and d_{002} is interlayer spacing. Fig. 3 (a) shows the diffraction peaks at 39.6º, 46.9º, 67.3º, 80.8º and 82.9º are related to (111), (200), (220), (311) and (222) planes of face-centered-cubic (*fcc*) Pt (JCPDS 04-0601), confirming that Pt precursor has been successfully reduced to Pt nanoparticles during the course of chemical reduction. The peak corresponding to the (111) plane is more intense than the others, indicating that the (111) plane is the dominating orientation. The average crystallite size for the Pt nanoparticles is calculated from broadening of the (111) diffraction peak using modified form of Scherrer equation.[65-67]

$$d = 0.9\lambda/\beta_{1/2}\cos\theta \qquad \text{(iii)}$$

where d is the average particle size (nm), λ is the wavelength of the X-ray used (1.54056 Å), θ is the angle at the maximum of the peak (rad), and $\beta_{1/2}$ is the width of the peak at half height in radians. The calculated average size of Pt nanoparticles on graphene is 9±0.5

View Article Online
DOI: 10.1039/C3TB20923G

nm, which is in closely matched with that obtained from FE-SEM and TEM images. Moreover, a broad peak at 2θ=27.5º is due to the (002) plane of the hexagonal structure of the graphene support, indicated that the nature of GNs doesn't alter after PtNPs functionalization. The XRD diffractogram of N-GNs/PtNPs is similar to that of GNs/PtNPs (Fig. 3b). For N-GNs/PtNPs, the interlayer spacing is about 3.41 Å, which is little bigger than that of reduced GNs (3.36 Å), may be due to the defects resulted from nitrogen doping. However, N-doping treatment process can not affect the layers of GNs.

3.4. Electrochemical oxidation of HCY at N-GNs/PtNPs nanocomposites electrode.

HCY is an important amino acid, which doesn't found directly in the diet but formed during methionine metabolism.[68] It has been documented that, HCY concentration in the blood plasma is approximately 5–16 μmol L^{-1}, and higher concentrations of HCY give rise to hyperhomocysteinemia (≤100 μmol L^{-1}) or homocystinuria (~500 μmol L^{-1}).[68] It has been known that, hyperhomocysteinemia is associated together with folate and cobalamine deficiencies, and also it leads to the early pregnancy loss, mental disorder and tumors.[69] Further, a moderate increase in HCY concentration is associated with an increase risk of coronary artery and cerebrovascular diseases[70] including atherosclerosis and thrombosis.[71] Further, ascorbic acid (AA) is always co-exists with HCY in our body fluids and further its concentration is very much higher when compared to HCY concentration. Since these biomolecules coexist in human fluids, their simultaneous determination is essential to secure the human health from the above critical diseases risk. Therefore, highly selective and sensitive determination of HCY is very important from the clinical and health viewpoints.

We have examined the electrocatalytic activity of N-GNs/PtNPs GC, GNs/PtNPs GC, GNs GC and unmodified GC electrodes towards the oxidation of HCY. We found that the N-GNs/PtNPs GC modified GC electrode showed higher electrocatalytic activity towards HCY

View Article Online
DOI: 10.1039/C3TB20923G

and AA than the other modified and unmodified GC electrodes. Fig. 4A shows the cyclic voltammograms (CVs) obtained for 0.2 mM HCY at N-GNs/PtNPs GC, GNs/PtNPs GC, GNs GC and bare GC electrodes in a 0.20 M phosphate buffer (PB) solution (pH=7.2). Bare GCE does not show any response for HCY in the potential window of -0.40 to 1.00 V (curve a), while the GNs modified electrode showed an oxidation wave for HCY at 0.63 V (curve b). Notably, the incorporation of PtNPs into GNs (GNs/PtNPs) have significantly increasing the oxidation current of HCY at the same potential (0.63 V; curve c). Interestingly, N-GNs/PtNPs modified GC electrode showed 210 mV less positive potential shift (i.e., oxidized 0.42 V) at and ~3-fold higher oxidation current for HCY (curve d) when compared to GNs/PtNPs modified electrode prepared under identical conditions (curve c). The observed oxidation potential (0.42 V) is comparably less positive oxidation potential compared to the previously reported polymer, polymer–nanoparticles and other chemically modified electrodes (references are listed in the supporting information). For a comparison, we performed oxidation of HCY by using N-GNs modified electrode (curve f) and observed that the oxidation potential of HCY shifted ~160 mV less positive potential; however the oxidation current density is increased in small amount compared to GNs/PtNPs. Thus the N-GNs/PtNPs composite nanomaterial is very important for developing an electrochemical HCY biosensor. The N-GNs/PtNPs electrode exhibited an enhanced electrocatalytic response of HCY mainly due to the following reasons. The incorporation of nitrogen into carbon materials, especially in the form of pyridinium moieties,[72] is critical for the enhancement of the electrocatalytic activity. Because the nitrogen atoms doped in graphene was formed dominative pyridinic N and pyrrolic N, in the nanocomposites. In addition, the nitrogen atom is inserted into the graphite plane, bonded to three carbon atoms and formed quaternary N, which referred as "graphitic nitrogen" (G-N).[39] As has been reported, nitrogen doping introduces atomic charge density and asymmetry in the spin density on the graphene network that facilitates the charge

View Article Online
DOI: 10.1039/C3TB20923G

transfer from the carbon support to the adsorbing molecules. Under near-physiological conditions (pH=7.2), HCY has an amino group $-NH_3^+$ and a carboxyl group $-CO_2^-$.[73, 74] At this point, the electrostatic interaction between negatively charged $-CO_2^-$ of HCY and positively charged pyridinium moieties of N-doped GNs/PtNPs showed higher oxidation current for HCY. It has been also implying that, the incorporated nitrogen atoms can enhance the interaction between carbon structure and metals, thus the kinetics of HCY diffusion and bio-sensing efficiency can be improved. Moreover, PtNPs have large specific active surface area and can act as tiny conducting centers, which was distributed throughout the GNs network and formed a continuous assembly of PtNPs on the surface, resulting that decrease the energy barrier, facilitate electron transfer, and improve biosensor response. It has been known that the thiol -(SH) and amino group ($-NH_3^+$) in HCY molecule have had the higher affinity on PtNPs in the nanocomposite through the Pt-S and interparticle binding through electrostatic interactions between amino groups, which access the more amount of biomolecule HCY on PtNPs surface by three-dimensional assembly (Scheme 2), as compared to the two-dimensional substrate. To understand the fast electron transfer reaction of HCY at N-GNs/PtNPs modified electrode quantitatively, we have calculated the standard heterogeneous rate constant (k_s) for HCY at N-GNs/PtNPs and other electrodes. The HCY oxidation is irreversible process and hence we have used Velasco equation (iv)[75] to calculate the heterogeneous rate constant (k_s):

$$k_s = 1.11 D_o^{1/2} (E_p - E_{p1/2})^{-1/2} \upsilon^{1/2} \text{..... (iv)}$$

where k_s is standard heterogeneous rate constant; D_o is apparent diffusion coefficient; E_p is oxidation peak potential; $E_{p/2}$ is half-wave oxidation peak potential and υ is the scan rate. In order to determine the k_s, it is essential to find the diffusion coefficient values for HCY. The D_o value was determined by a single step potential chronoamperometry method based on the

View Article Online
DOI: 10.1039/C3TB20923G

Cottrell slope obtained[76] by plotting current versus 1/√time. The chronoamperometry measurements were performed for HCY at GNs, GNs/PtNPs and N-GNs/PtNPs modified electrodes after 20 potential cycles and obtained D_o values were of 2.85×10^{-5} cm^2 s^{-1}, 4.96×10^{-5} cm^2 s^{-1} and 8.12×10^{-5} cm^2 s^{-1} for GNs, GNs/PtNPs and N-GNs/PtNPs modified GC electrodes, respectively. The estimated k_s values for the oxidation of HCY at GNs, GNs/PtNPs and N-GNs/PtNPs modified GC electrodes were found to be 1.84×10^{-3}, 3.27×10^{-3} and 8.74×10^{-3} cms^{-1}, respectively. Since the bare GC electrode was failed to oxidize the HCY and thus the k_s value was not obtained for bare GC electrode . The obtained higher k_s value for HCY at N-GNs/PtNPs modified electrode indicated that the oxidation of HCY was faster at N-GNs/PtNPs modified electrode than the GNs/PtNPs, GNs and bare GC electrodes. Further, we have recorded linear sweep voltammograms (LSVs) at different scan rates to know whether the oxidation of HCY at N-GNs/PtNPs modified electrode is due to diffusion control or adsorption. The oxidation peak current of HCY increased while increasing the scan rate (Fig. 4B). A good linearity between the anodic peak current and the square root of the scan rate with a correlation coefficient of 0.9910 was obtained within the range of 25-250 mVs^{-1}. This indicated that the electrode reaction of HCY was under diffusion controlled process.

3.5. Simultaneous determination of HCY and AA. It is essential to determine HCY in the presence of AA because it is one of the main interferents for the determination of HCY. The CVs obtained for a mixture of 0.2 mM each HCY and AA at bare GC, GNs, GNs/PtNPs and N-GNs/PtNPs modified electrodes in 0.2 M PB solution (pH=7.20) were shown in Fig. 5. The bare GC electrode fails to separate the voltammetric signals of AA and HCY as evidenced from the mixed voltammetric wave around 0.27 V (curve a). However, GNs modified electrode resolves the oxidation peaks of HCY and AA at 0.65 and 0.05 V with a

View Article Online
DOI: 10.1039/C3TB20923G

potential difference of 600 mV (curve b). Then, the incorporation of PtNPs into GNs have significantly increasing the oxidation current of both HCY and AA (curve c) at same potential. Interestingly, N-GNs/PtNPs modified electrode oxidizes HCY and AA at 0.50 and -0.12 V, respectively. It has been explain that the N-GNs/PtNPs modified electrode showed nearly 3-fold-enhancement in the oxidation current of HCY and AA, and significantly reduced the oxidation over potential is about ~160 mV than GNs/PtNPs modified electrode. In addition, the oxidation peaks of both HCY and AA were highly stable even after 20 cycles as evidenced in curve e. The N-GNs/PtNPs modified electrode did not show any voltammetric response in the absence of HCY and AA (curve f). Further, this N-GNs/PtNPs modified electrode showed a very large peak separation (620 mV) between AA and HCY at physiological pH. Usually higher concentration of AA co-exists with HCY in our body fluids, therefore it is highly essential to determine HCY in the presence of higher concentration of AA. The differential pulse voltammograms (DPVs) obtained for the oxidation of 10 μM HCY in the presence of 0.2 mM AA is shown in Fig. 6. A clear voltammetric signal was observed for HCY even in the presence of 20-fold excess of AA (curve b). Addition of each 10 μM HCY to 0.2 mM AA in PB solution increases the current due to the oxidation of HCY while the peak current due to AA was unchanged. The observed results indicate that N-GNs/PtNPs modified electrode is more sensitive towards the oxidation HCY even in the presence of higher concentration of AA (20-fold excess). The oxidation peak currents of HCY linearly increased in each 10 μM addition of HCY with a correlation coefficient of 0.9951. On the other hand, we have tested the same experiment for GNs/PtNPs modified electrode and it doesn't show enhanced signal for HCY in presence of AA (Supporting Information ESI Fig. S1).

View Article Online
DOI: 10.1039/C3TB20923G

3.6. Amperometric determination of HCY. The sensitivity of N-GNs/PtNPs modified electrode to HCY was analyzed by using constant potential amperometry under steady state conditions. Fig. 7A depicts the amperometric *i–t* curve obtained for the oxidation of HCY at the N-GNs/PtNPs modified electrode in a constantly stirred 0.2 M PB solution at an applied potential of +0.60 V. An initial steady-state amperometric current response was observed due to the addition of 2 nM HCY, and then the addition of 2 nM HCY in each step with a sample interval of 50 s, the current response linearly increases and a steady state current response was obtained within 2 s which indicates a fast electron-transfer process at this electrode. We found that 2.40 nA current was obtained for single addition of 2 nM HCY (1.35 nA/nM) at N-GNs/PtNPs electrode. The observed stable amperometric current response with higher sensitivity of HCY at N-GNs/PtNPs modified electrode indicated that this electrode can be successfully used for the sensitive detection of 2 nM HCY. The amperometric current responses increased linearly with HCY concentration from 2 to 24 nM (Fig. 7A; curve a) and the calibration plot obtained for amperometric current responses versus various concentrations of HCY is shown in inset of Fig. 7A. A good linearity was obtained with a correlation coefficient of 0.9970 in the concentration range was used in Fig. 7. For comparison, the sensitivity of GNs/PtNPs modified electrode towards HCY was examined by amperometry and the sensitivity limit was found to be 0.6 nA/nM (Fig. 7 curve b). Moreover, we have observed amperometric signals in picomolar concentrations of HCY, which is shown in Fig. 7B. The N-GNs/PtNPs electrode was polarized at +0.60 V, and aliquots of HCY were injected into a stirred electrolyte solution. A rapid increase in the current was noticed after each addition of 200 pM HCY into the electrolyte solution, and a steady state response was attained within 2 s. Thus the experimental detection limit of present N-GNs/PtNPs modified electrode was calculated as 200 pM. The N-GNs/PtNPs electrode is highly sensitive, and the amperometric response is very stable and offers a linear dependence over a wide range of

View Article Online
DOI: 10.1039/C3TB20923G

HCY concentrations (~1 mM). The observed results indicate that N-GNs/PtNPs modified electrode showed higher sensitivity than GNs/PtNPs modified electrode. It is worth to compare the performance of the N-GNs/PtNPs modified electrode towards HCY with those of recently reported polymer, polymer–nanoparticles and other chemically modified electrodes. We summarized the limit of detections with relevant references in supporting information Table S1. Our limit of detection is very low (200 pM), compared the reports available in the literature based on electrochemical HCY biosensors. In our system, PtNPs were embedded by three dimensionally on the surface nitrogen doped GNs leads to the formation of more electroactive graphene layers and electrostatic interactions between HCY and the three dimensionally formed N-GNs/PtNPs, which offers high performance platform toward the detection of HCY.

3.7. Effect of interferents. We have studied the determination of HCY in the presence of common interferents such as glucose, urea, uric acid, serotonin and oxalate by amperometric method. The amperometric *i–t* curve obtained for HCY at N-GNs/PtNPs modified electrode in the presence common interferents (Fig. 8) in a constantly stirred 0.2 M PB solution (pH=7.2) at a constant applied potential of +0.60 V. The increased initial current response was due to the addition of 2 nM HCY (a) and further addition of 2 nM HCY in each step with a sample interval of 50 s, the current response increases and a steady state current response was attained within 2 s (a, b, and c). After three steps (a, b, and c), the addition of 1 μM each glucose (d), urea (e) and uric acid (f) separately with a sample interval of 50 s to the same 0.2 M PB solution (pH=7.2), no change in amperometric current response was observed. However, again the addition of 2 nM HCY to the same solution (g, h, i and j), the current response was again increased almost similar to steps a, b, and c. After four steps (g, h, i and j), again the addition of 1 μM each serotonin (k), oxalate (l) and thiourea (m) separately

View Article Online
DOI: 10.1039/C3TB20923G

with a sample interval of 50 s to the same 0.2 M PB solution (pH=7.2), similar amperometric current response was observed (steps d-e). Finally, the addition of 2 nM HCY to the same solution (n and o), the current response was again increased almost similar to the steps "a-c" and "g-j". Similarly, the selectivity of HCY was also studied in the presence of some other important bio-molecules (interferences) such as dopamine, epinephrine and L-dopa (Fig. S2 in Supporting Information); the N-GNs/PtNPs modified electrode was highly selective toward the determination of HCY in presence of important bio-molecules. The observed result indicates that N-GNs/PtNPs modified electrode can be successfully used for the determination of 2 nM HCY even in the presence of 500-fold excess of several common interferents.

3.8. Stability and reproducibility. The long-term storage and operational stability of the electrode is essential for the continuous monitoring of HCY. The stability of the present electrode was examined by using the same N-GNs/PtNPs modified electrode for 20 repetitive measurements in a supporting electrolyte solution containing 0.2 mM HCY. The electrode used in this measurement was kept in 0.2 M PB solution and was subjected to another 20 repetitive measurements after 12 and 24 h. We observed that no noticeable change in the peak potential and peak current for the oxidation of HCY in both sets of experiments. The coefficient of variation was calculated separately for the two sets of experiments and we found that it remained the same (0.52 and 0.63%) in both sets. This shows that the electrode is stable and does not undergo poisoning by the oxidation products, and can be used for the repeated measurement of HCY. To further ascertain the operational stability of the present electrode, voltammetric measurement in a supporting electrolyte solution containing 0.2 mM HCY was performed with the N-GNs/PtNPs electrode and the peak current for the oxidation of HCY was measured at regular intervals over a period of 25 h. As shown in Fig.9, the

View Article Online
DOI: 10.1039/C3TB20923G

magnitude of the peak current did not change appreciably during the whole set of experiments (25 h), demonstrating that the N-GNs/PtNPs electrode is very stable and retains its sensitivity throughout the experiments. To check the long-term storage stability of the present HCY sensor, the N-GNs/PtNPs modified electrode was kept in 0.2 M PB solution (pH = 7.2) at room temperature. No appreciable decrease in the oxidation current response of HCY was observed for 4 days, and the current decreased by only 2.8% after two weeks. To ascertain the reproducibility of the results, two different GC electrodes were modified with the N-GNs/PtNPs in the same way and each electrode response towards 0.2 mM HCY was tested by 10 repeated measurements. The peak current obtained for the two independent electrodes again showed an RSD of 0.8%, confirming that the results were highly reproducible.

3.9. Determination of HCY in real sample analysis. The practical application of N-GNs/PtNPs modified electrode for the determination of HCY in real samples was tested by measuring the concentration of HCY in human blood serum and urine samples. The human urine samples were diluted to 100-fold in 0.2 M PB solution without any other treatment, which could reduce the matrix effect of real samples. The DPV obtained for N-GNs/PtNPs modified electrode in 0.5 ml of the human blood serum sample in 9.5 ml of 0.2 M PB solution is shown as line “a” in Fig. 10A. It shows a oxidation peak at 0.45 V, which is attributed to the oxidation of HCY. To confirm the observed oxidation peak was due to HCY, the sample was spiked with 20 μM commercial HCY and the resulting DPV is shown as line “b” in Fig. 10A. An increase in the peak current confirmed that the oxidation peak at 0.45V (line a) was due to the oxidation of HCY. The DPV experiment was done for four samples of human serum samples and the results are given in Table S2. The recovery rates of the spiked samples were 99.8, 99.8, 99.7 and 99.6% for the three samples of human blood serum (Table

View Article Online
DOI: 10.1039/C3TB20923G

S2). In addition to human blood serum sample, the application of the electrode was extended to the measurement of HCY in human urine sample. The curve "a" in Fig. 10B shows the DPV obtained for 10 ml of diluted human urine sample in 0.2 M PB solution. A broad oxidation peak was observed at 0.48 V, which is attributed to the oxidation of HCY. To confirm the observed oxidation peak was due to the oxidation of HCY, the sample was spiked with 20 μM commercial HCY and the resulting DPV is shown as curve "b" in Fig. 10B. An increase in the peak current confirmed that the oxidation peak at 0.48V (curve b) was due to the oxidation of HCY. The results obtained in the present study illustrate that the N-GNs/PtNPs modified electrode is highly suitable for the determination of HCY in human blood serum and urine samples.

4. Conclusions

We demonstrated the synthesis of nitrogen doped graphene supported PtNPs (N-GNs/PtNPs) as graphene based nanocomposites for high performance electrocatalyst toward electrochemical oxidation of homocysteine (HCY). Our investigation demonstrate that, N-doped graphene supported PtNPs showed higher electrocatalytic catalytic activity of HCY with an experimental detection limit of 200 pM. In addition, the N-doped graphene supported PtNPs nanocomposites demonstrated as an excellent selectivity in the electrochemical oxidation of HCY i.e., the detection of HCY is successful in the presence of ascorbic acid (AA) and other important interferents. The practical application of N-GNs/PtNPs nanocomposite was successfully used for the determination of HCY in both human blood serum and urine samples by differential pulse voltammetry under optimized conditions. Our findings conclude that N-GNs/PtNPs nanocomposite can be developed as an efficient and versatile high performance electrocatalyst for electrochemical biosensor applications.

Acknowledgements

View Article Online
DOI: 10.1039/C3TB20923G

Palanisamy Kannan and Marcin Opallo thank **N**an**O**technology **B**iomaterials and a**L**ternative **E**nergy **S**ource for **E**RA Integration [FP7-REGPOT-CT-2011-285949-NOBLESSE] Project from European Union.

References

1. A. J. Patil, J. L. Vickery, T. B. Scott and S. Mann, *Advanced Materials*, 2009, **21**, 3159-3164.
2. C.-H. Lu, H.-H. Yang, C.-L. Zhu, X. Chen and G.-N. Chen, *Angewandte Chemie International Edition*, 2009, **48**, 4785-4787.
3. N. Mohanty and V. Berry, *Nano Letters*, 2008, **8**, 4469-4476.
4. M. Zhou, Y. Zhai and S. Dong, *Analytical Chemistry*, 2009, **81**, 5603-5613.
5. Y. Wang, J. Lu, L. Tang, H. Chang and J. Li, *Analytical Chemistry*, 2009, **81**, 9710-9715.
6. C. Shan, H. Yang, J. Song, D. Han, A. Ivaska and L. Niu, *Analytical Chemistry*, 2009, **81**, 2378-2382.
7. Y. Shao, J. Wang, H. Wu, J. Liu, I. A. Aksay and Y. Lin, *Electroanalysis*, 2010, **22**, 1027-1036.
8. X. Li, G. Zhang, X. Bai, X. Sun, X. Wang, E. Wang and H. Dai, *Nat Nano*, 2008, **3**, 538-542.
9. A. K. Geim and K. S. Novoselov, *Nat Mater*, 2007, **6**, 183-191.
10. H. Huang, S. Chen, X. Gao, W. Chen and A. T. S. Wee, *ACS Nano*, 2009, **3**, 3431-3436.
11. RamanathanT, A. A. Abdala, StankovichS, D. A. Dikin, M. Herrera Alonso, R. D. Piner, D. H. Adamson, H. C. Schniepp, ChenX, R. S. Ruoff, S. T. Nguyen, I. A. Aksay, R. K. Prud'Homme and L. C. Brinson, *Nat Nano*, 2008, **3**, 327-331.
12. J. L. Vickery, A. J. Patil and S. Mann, *Advanced Materials*, 2009, **21**, 2180-2184.
13. H. Wang, T. Maiyalagan and X. Wang, *ACS Catalysis*, 2012, **2**, 781-794.
14. H. M. Jeong, J. W. Lee, W. H. Shin, Y. J. Choi, H. J. Shin, J. K. Kang and J. W. Choi, *Nano Letters*, 2011, **11**, 2472-2477.
15. Y. Ma, A. S. Foster, A. V. Krasheninnikov and R. M. Nieminen, *Physical Review B*, 2005, **72**, 205416.
16. C. Zhou, J. Kong, E. Yenilmez and H. Dai, *Science*, 2000, **290**, 1552-1555.
17. T. O. Wehling, K. S. Novoselov, S. V. Morozov, E. E. Vdovin, M. I. Katsnelson, A. K. Geim and A. I. Lichtenstein, *Nano Letters*, 2007, **8**, 173-177.
18. L. Liu, S. Ryu, M. R. Tomasik, E. Stolyarova, N. Jung, M. S. Hybertsen, M. L. Steigerwald, L. E. Brus and G. W. Flynn, *Nano Letters*, 2008, **8**, 1965-1970.
19. G. Giovannetti, P. A. Khomyakov, G. Brocks, V. M. Karpan, J. van den Brink and P. J. Kelly, *Physical Review Letters*, 2008, **101**, 026803.
20. S. U. Lee, R. V. Belosludov, H. Mizuseki and Y. Kawazoe, *Small*, 2009, **5**, 1769-1775.
21. L. L. Zhang, X. Zhao, H. Ji, M. D. Stoller, L. Lai, S. Murali, S. McDonnell, B. Cleveger, R. M. Wallace and R. S. Ruoff, *Energy & Environmental Science*, 2012, **5**, 9618-9625.
22. F. Su, C. K. Poh, J. S. Chen, G. Xu, D. Wang, Q. Li, J. Lin and X. W. Lou, *Energy & Environmental Science*, 2011, **4**, 717-724.
23. K. Xiao, Y. Liu, P. a. Hu, G. Yu, Y. Sun and D. Zhu, *Journal of the American Chemical Society*, 2005, **127**, 8614-8617.
24. E. P. Randviir and C. E. Banks, *RSC Advances*, 2012, **2**, 5800-5805.
25. D. A. C. Brownson, C. W. Foster and C. E. Banks, *Analyst*, 2012, **137**, 1815-1823.
26. X. Wang, X. Li, L. Zhang, Y. Yoon, P. K. Weber, H. Wang, J. Guo and H. Dai, *Science*, 2009, **324**, 768-771.
27. P. Wu, Z. Cai, Y. Gao, H. Zhang and C. Cai, *Chemical Communications*, 2011, **47**, 11327-11329.

View Article Online
DOI: 10.1039/C3TB20923G

28. D. Usachov, O. Vilkov, A. Grüneis, D. Haberer, A. Fedorov, V. K. Adamchuk, A. B. Preobrajenski, P. Dudin, A. Barinov, M. Oehzelt, C. Laubschat and D. V. Vyalikh, *Nano Letters*, 2011, **11**, 5401-5407.
29. L. Qu, Y. Liu, J.-B. Baek and L. Dai, *ACS Nano*, 2010, **4**, 1321-1326.
30. A. L. M. Reddy, A. Srivastava, S. R. Gowda, H. Gullapalli, M. Dubey and P. M. Ajayan, *ACS Nano*, 2010, **4**, 6337-6342.
31. Z.-J. Lu, S.-J. Bao, Y.-T. Gou, C.-J. Cai, C.-C. Ji, M.-W. Xu, J. Song and R. Wang, *RSC Advances*, 2013, **3**, 3990-3995.
32. H. Yin, H. Tang, D. Wang, Y. Gao and Z. Tang, *ACS Nano*, 2012, **6**, 8288-8297.
33. J. Lu, I. Do, L. T. Drzal, R. M. Worden and I. Lee, *ACS Nano*, 2008, **2**, 1825-1832.
34. S. Guo, D. Wen, Y. Zhai, S. Dong and E. Wang, *ACS Nano*, 2010, **4**, 3959-3968.
35. V. B. Parambhath, R. Nagar and S. Ramaprabhu, *Langmuir*, 2012, **28**, 7826-7833.
36. B. P. Vinayan, K. Sethupathi and S. Ramaprabhu, *International Journal of Hydrogen Energy*, 2013, **38**, 2240-2250.
37. W. S. Hummers and R. E. Offeman, *Journal of the American Chemical Society*, 1958, **80**, 1339-1339.
38. L. Sun, L. Wang, C. Tian, T. Tan, Y. Xie, K. Shi, M. Li and H. Fu, *RSC Advances*, 2012, **2**, 4498-4506.
39. Y. Wang, Y. Shao, D. W. Matson, J. Li and Y. Lin, *ACS Nano*, 2010, **4**, 1790-1798.
40. Y. Xu, L. Zhao, H. Bai, W. Hong, C. Li and G. Shi, *Journal of the American Chemical Society*, 2009, **131**, 13490-13497.
41. D. Barun, K. E. Prasad, U. Ramamurty and C. N. R. Rao, *Nanotechnology*, 2009, **20**, 125705.
42. S. Ghosh and C. R. Raj, *The Journal of Physical Chemistry C*, 2010, **114**, 10843-10849.
43. Y. Li, W. Gao, L. Ci, C. Wang and P. M. Ajayan, *Carbon*, 2010, **48**, 1124-1130.
44. D. Deng, X. Pan, L. Yu, Y. Cui, Y. Jiang, J. Qi, W.-X. Li, Q. Fu, X. Ma, Q. Xue, G. Sun and X. Bao, *Chemistry of Materials*, 2011, **23**, 1188-1193.
45. B. Xiong, Y. Zhou, R. O'Hayre and Z. Shao, *Applied Surface Science*, 2013, **266**, 433-439.
46. J. Yang, C. Tian, L. Wang and H. Fu, *Journal of Materials Chemistry*, 2011, **21**, 3384-3390.
47. Z. Zheng, Y. Du, Z. Wang, Q. Feng and C. Wang, *Analyst*, 2013, **138**, 693-701.
48. K. Vinodgopal, B. Neppolian, I. V. Lightcap, F. Grieser, M. Ashokkumar and P. V. Kamat, *The Journal of Physical Chemistry Letters*, 2010, **1**, 1987-1993.
49. G. Goncalves, P. A. A. P. Marques, C. M. Granadeiro, H. I. S. Nogueira, M. K. Singh and J. Grácio, *Chemistry of Materials*, 2009, **21**, 4796-4802.
50. D. Yang, A. Velamakanni, G. Bozoklu, S. Park, M. Stoller, R. D. Piner, S. Stankovich, I. Jung, D. A. Field, C. A. Ventrice Jr and R. S. Ruoff, *Carbon*, 2009, **47**, 145-152.
51. D.-H. Lim and J. Wilcox, *The Journal of Physical Chemistry C*, 2011, **115**, 22742-22747.
52. D.-Q. Yang and E. Sacher, *The Journal of Physical Chemistry C*, 2008, **112**, 4075-4082.
53. A. S. Aricò, A. K. Shukla, H. Kim, S. Park, M. Min and V. Antonucci, *Applied Surface Science*, 2001, **172**, 33-40.
54. W. Eberhardt, P. Fayet, D. M. Cox, Z. Fu, A. Kaldor, R. Sherwood and D. Sondericker, *Physical Review Letters*, 1990, **64**, 780-783.
55. S. Hüfner and G. K. Wertheim, *Physical Review B*, 1975, **11**, 678-683.
56. D. Wei, Y. Liu, Y. Wang, H. Zhang, L. Huang and G. Yu, *Nano Letters*, 2009, **9**, 1752-1758.
57. J. W. Jang, C. E. Lee, S. C. Lyu, T. J. Lee and C. J. Lee, *Applied Physics Letters*, 2004, **84**, 2877-2879.
58. C. Ronning, H. Feldermann, R. Merk, H. Hofsäss, P. Reinke and J. U. Thiele, *Physical Review B*, 1998, **58**, 2207-2215.
59. D. Marton, K. J. Boyd, A. H. Al-Bayati, S. S. Todorov and J. W. Rabalais, *Physical Review Letters*, 1994, **73**, 118-121.

View Article Online
DOI: 10.1039/C3TB20923G

60. X. Wang, Y. Liu, D. Zhu, L. Zhang, H. Ma, N. Yao and B. Zhang, *The Journal of Physical Chemistry B*, 2002, **106**, 2186-2190.
61. J. Casanovas, J. M. Ricart, J. Rubio, F. Illas and J. M. Jiménez-Mateos, *Journal of the American Chemical Society*, 1996, **118**, 8071-8076.
62. C. Jin, T. C. Nagaiah, W. Xia, B. Spliethoff, S. Wang, M. Bron, W. Schuhmann and M. Muhler, *Nanoscale*, 2010, **2**, 981-987.
63. Y. Xu, H. Bai, G. Lu, C. Li and G. Shi, *Journal of the American Chemical Society*, 2008, **130**, 5856-5857.
64. S. Park, J. An, I. Jung, R. D. Piner, S. J. An, X. Li, A. Velamakanni and R. S. Ruoff, *Nano Letters*, 2009, **9**, 1593-1597.
65. R. K. Srivastava, S. Srivastava, T. N. Narayanan, B. D. Mahlotra, R. Vajtai, P. M. Ajayan and A. Srivastava, *ACS Nano*, 2011, **6**, 168-175.
66. B. Sakintuna, Y. Yürüm and S. Çetinkaya, *Energy & Fuels*, 2004, **18**, 883-888.
67. S. Srivastava, V. Kumar, M. A. Ali, P. R. Solanki, A. Srivastava, G. Sumana, P. S. Saxena, A. G. Joshi and B. D. Malhotra, *Nanoscale*, 2013, **5**, 3043-3051.
68. M. Á. Medina, J. L. Urdiales and M. I. Amores-Sánchez, *European Journal of Biochemistry*, 2001, **268**, 3871-3882.
69. W. L. D. M. Nelan, H. J. Blom, E. A. P. Steegers, M. Den Heijer, C. M. G. Thomas and T. K. A. B. Eskes, *Obstetrics & Gynecology*, 2000, **95**, 519-524.
70. Biasioli. S and Schiavon. R, *Blood Purification*, 2000, **18**, 177-182.
71. M. M. Rees and G. M. Rodgers, *Thrombosis Research*, 1993, **71**, 337-359.
72. G. Yang, Y. Li, R. K. Rana and J.-J. Zhu, *Journal of Materials Chemistry A*, 2013, **1**, 1754-1762.
73. I. I. S. Lim, W. Ip, E. Crew, P. N. Njoki, D. Mott, C.-J. Zhong, Y. Pan and S. Zhou, *Langmuir*, 2006, **23**, 826-833.
74. J.-M. Zen, A. S. Kumar and J.-C. Chen, *Analytical Chemistry*, 2001, **73**, 1169-1175.
75. J. G. Velasco, *Electroanalysis*, 1997, **9**, 880-882.
76. A. J. Bard and R. W. Faulkner, *Electrochemical Methods, Fundamentals and Applications,*, 2001, 2nd ed. New York, Wiley.

View Article Online
DOI: 10.1039/C3TB20923G

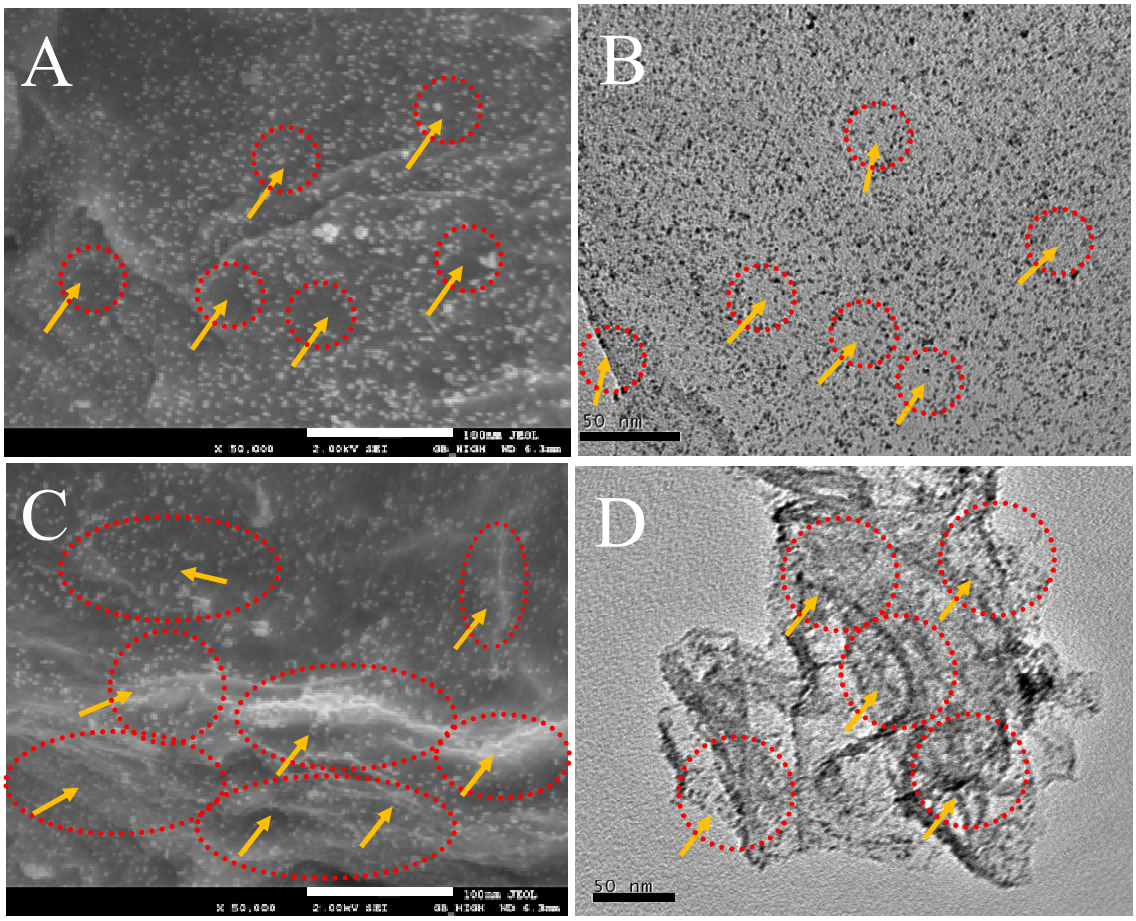

Fig. 1 FE-SEM images of GNs/PtNPs (A), and nitrogen doped GNs/PtNPs (C). The corresponding high resolution TEM images shown in (B) and (D) respectively. A uniform dispersion of PtNPs on GNs support is clearly visible. The arrow marks indicated that before and after nitrogen doping into the GNs/PtNPs nanocomposites. The scale bar is 100 nm (a and c); 50 nm (b and d).

View Article Online
DOI: 10.1039/C3TB20923G

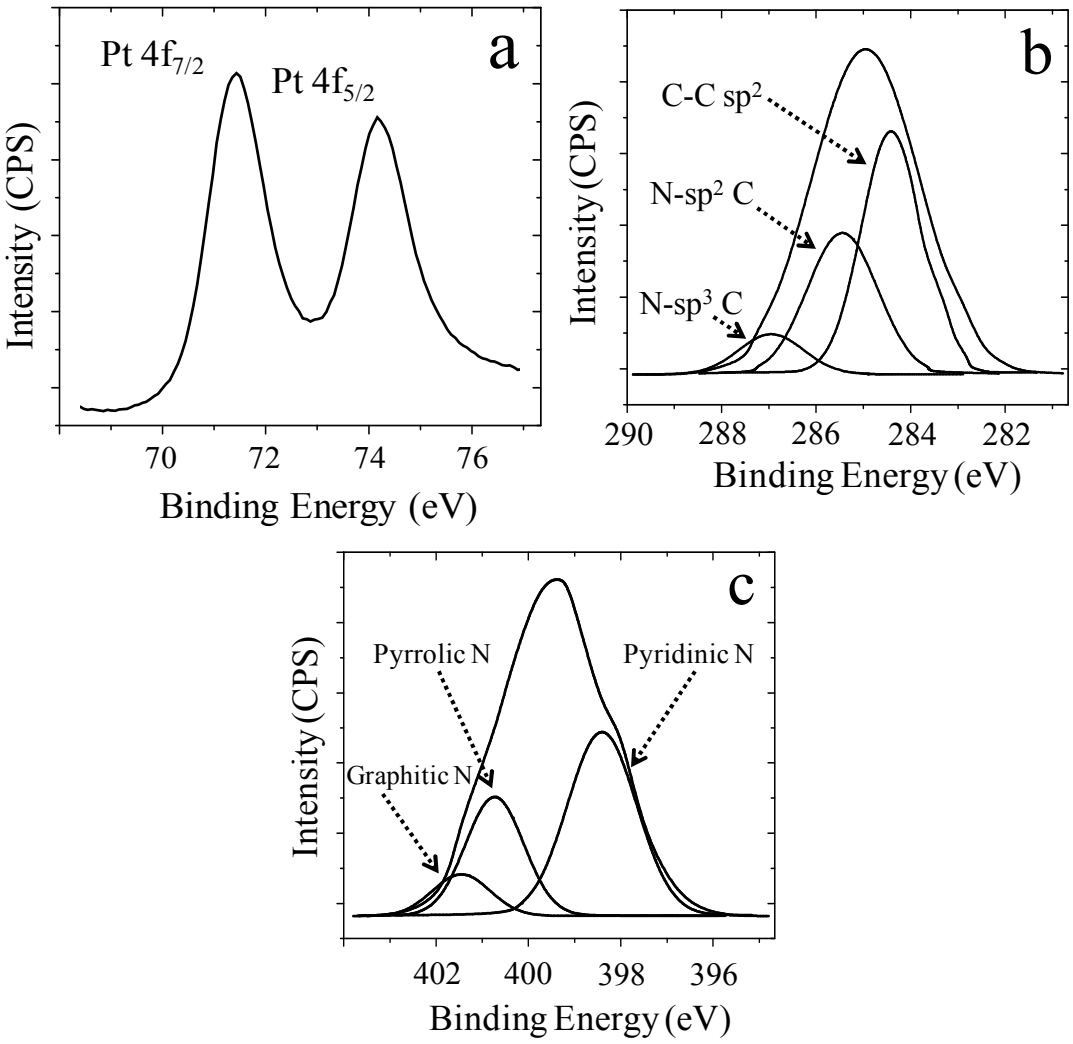

Fig. 2 Core level XPS spectra of (a) Pt (4f), (b) C1s, and (c) N1s orbitals of nitrogen doped GNs/PtNPs nanocomposites.

View Article Online
DOI: 10.1039/C3TB20923G

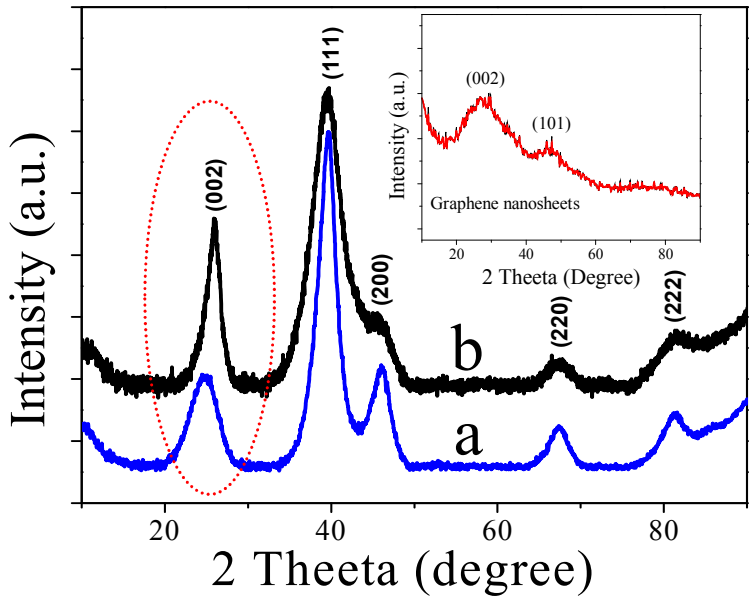

Fig. 3 XRD patterns of Pt/GNs (a) and N-GNs/PtNPs nanocomposites (b). Inset is XRD pattern of graphene nanosheets.

View Article Online
DOI: 10.1039/C3TB20923G

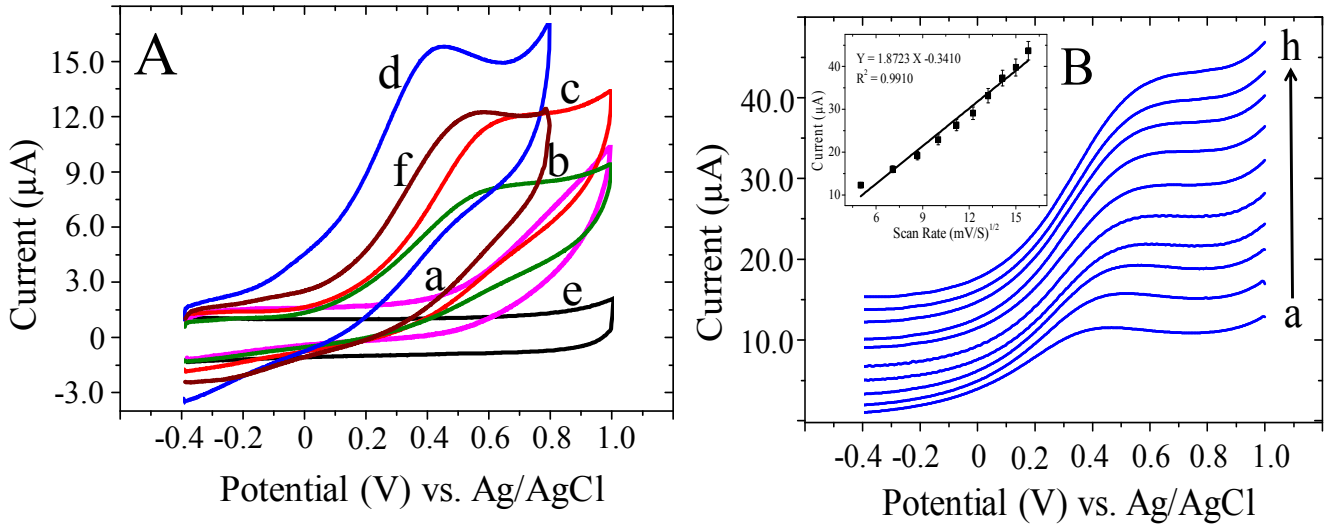

Fig. 4 (A) CVs obtained for 0.2 mM HCY at (a) bare GC, (b) GNs, (c) GNs/PtNPs and (d) N-GNs/PtNPs modified GC electrodes in 0.2 M PB solution (pH=7.2 N-GNs) at a scan rate of 50 mVs^{-1}. (e) CV of N-GNs/PtNPs modified GC electrode in the absence of 0.2 mM HCY. (f) CV of N-GNs modified GC electrode toward the oxidation of HCY. (B) Linear sweep voltammograms (LSVs) obtained for 0.2 mM HCY at N-GNs/PtNPs modified electrode in 0.2 M PB solution at different scan rates: (a) 25, (b) 50, (c) 75, (d) 100, (e) 125, (f) 150, (g) 175, (h) 200, (i) 225 and (j) 250 mVs^{-1}. The inset calibration plot is obtained for square root of the scan rate vs. anodic oxidation current of HCY.

View Article Online
DOI: 10.1039/C3TB20923G

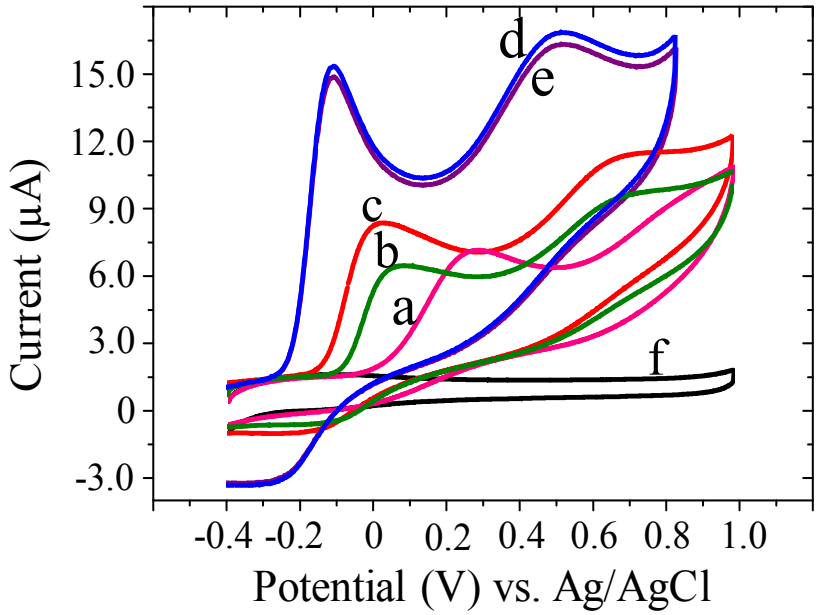

Fig. 5 CVs obtained for a mixture of 0.2 mM each HCY and AA at (a) bare GC, (b) GNs, (c) GNs/PtNPs and N-GNs/PtNPs (d) modified GC electrodes in 0.2 M PB solution (pH=7.2) at a scan rate of 50 mV s^{-1}. Curve (e) corresponding to the CV of N-GNs/PtNPs modified GC electrode after 20th measurement and (f) is the CV of N-GNs/PtNPs modified GC electrode in the absence of each 0.2 mM HCY and AA.

View Article Online
DOI: 10.1039/C3TB20923G

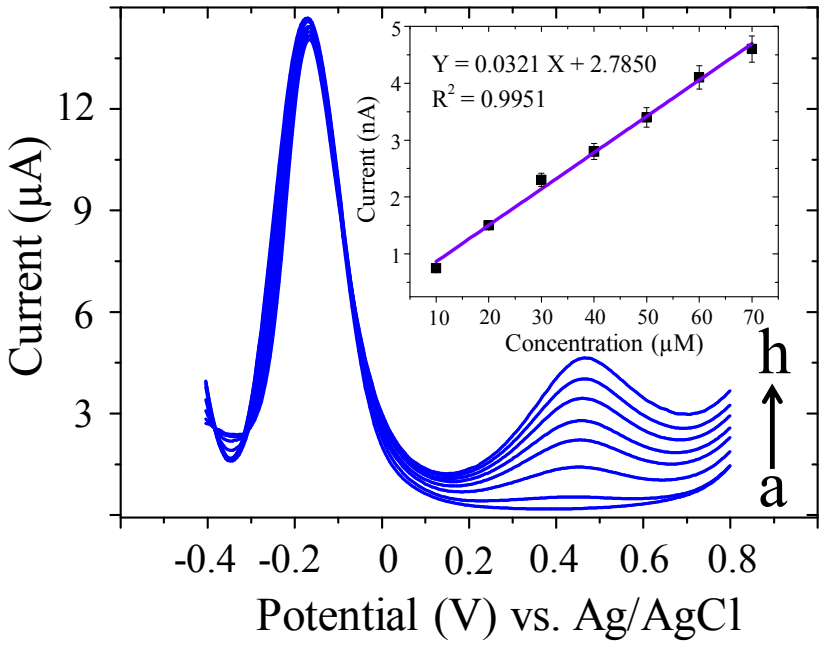

Fig. 6 DPVs for the oxidation of HCY at N-GNs/PtNPs modified GC electrode in different concentrations (a) 0, (b) 10, (c) 20, (d) 30, (e) 40, (f) 50, (g) 60, and (h) 70 μM in the presence of 0.2 mM of AA in 0.2 M PB solution. Pulse width = 0.05 s, amplitude = 0.05 V, sample period = 0.02 s and pulse period = 0.2 s. Inset: calibration plot is obtained for concentration of HCY vs. anodic oxidation currents.

View Article Online
DOI: 10.1039/C3TB20923G

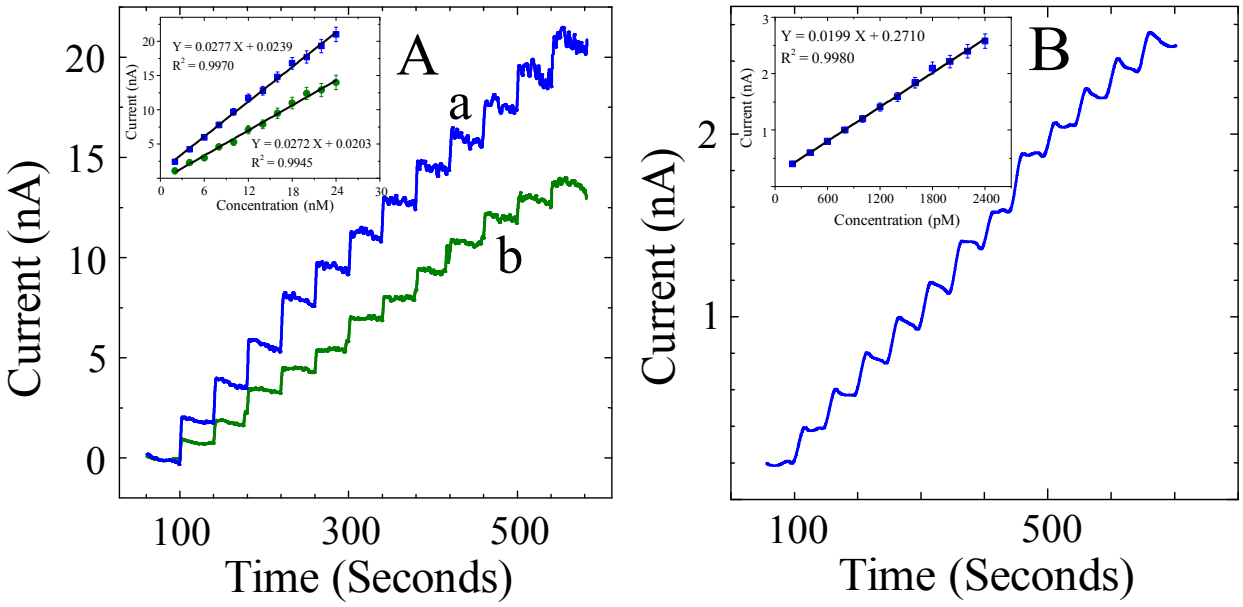

Fig. 7 (A) Amperometric *i–t* curves for each addition of 2 nM HCY at N-GNs/PtNPs (a) and GNs/PtNPs (b) modified GC electrodes in 0.2 M PB solution (pH=7.2) at a regular time interval of 50 s. (B) The N-GNs/PtNPs electrode vs. 200 pM of HCY into the stirred PB solution at regular time interval 0f 50 s. The electrode was polarized at +0.60 V. The inset shows corresponding calibration plot.

View Article Online
DOI: 10.1039/C3TB20923G

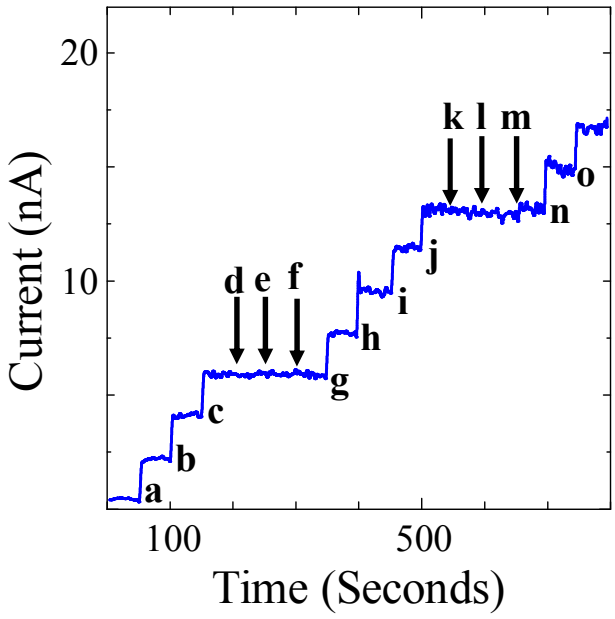

Fig. 8 Amperometric *i–t* curve responses (at a constant working potential of +0.60 V vs Ag/AgCl) obtained for 2 nM HCY (a, b and c) and 1 μM of glucose (d), urea (e) and uric acid (f), then each addition was made for 2 nM HCY (g, h, i and j), further step was the interference addition, 1 μM serotonin, oxalate and thiourea (k, l and m), and then final addition was made for 2 nM HCY (n and o) at N-GNs/PtNPs modified GC electrode in 0.2 M PB solution (pH=7.2) at a regular interval time of 50 s.

View Article Online
DOI: 10.1039/C3TB20923G

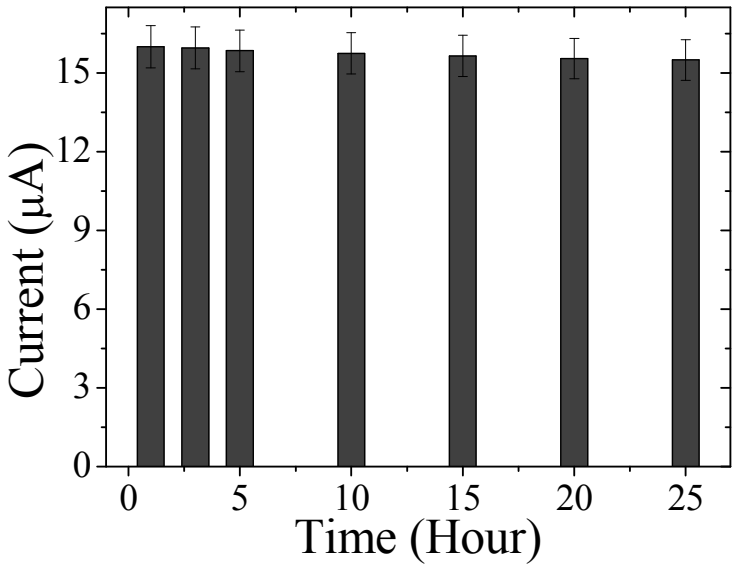

Fig.9 Plot of current versus time for the oxidation of HCY (0.2 mM) at N-GNs/PtNPs electrode in 0.2 M PB solution demonstrating the operational stability of the electrode.

View Article Online
DOI: 10.1039/C3TB20923G

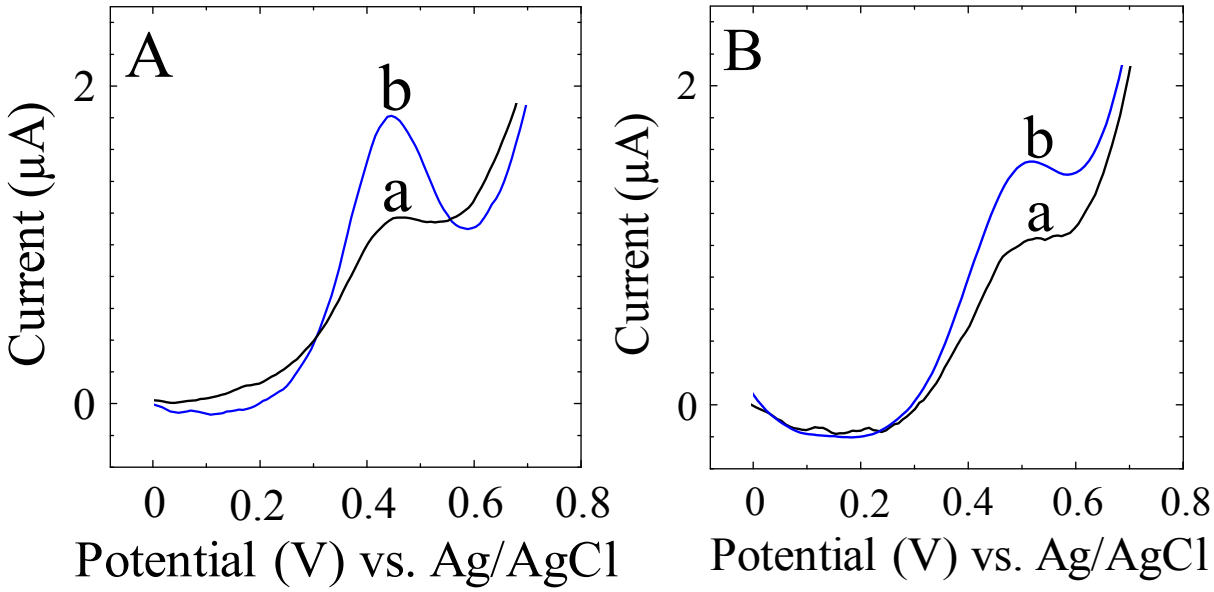

Fig. 10 (A) DPVs obtained for (a) human blood serum and (b) after the addition of 20 μM commercial HCY to human blood serum at N-GNs/PtNPs modified electrode in 0.2 M PB solution. (B) DPVs obtained for (a) human urine and (b) after the addition of 20 μM commercial HCY to human urine at N-GNs/PtNPs modified electrode in 0.2 M PB solution from 0 to 0.70 V. Pulse width = 0.05 s, amplitude = 0.05 V, sample period = 0.02 s and pulse period = 0.2 s.

View Article Online
DOI: 10.1039/C3TB20923G

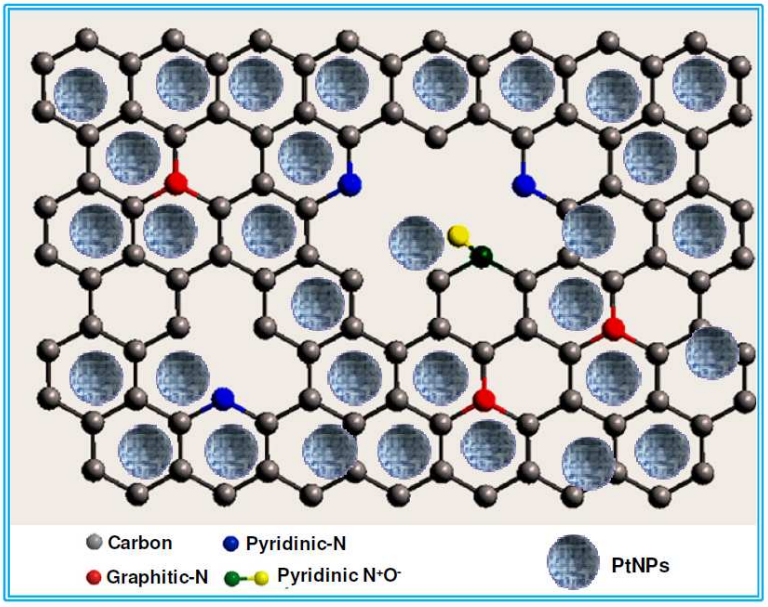

Scheme 1. Schematic of nitrogen-doped GNs/PtNPs depicting the nature of bonding of nitrogen atoms in the graphene nanosheets.

View Article Online
DOI: 10.1039/C3TB20923G

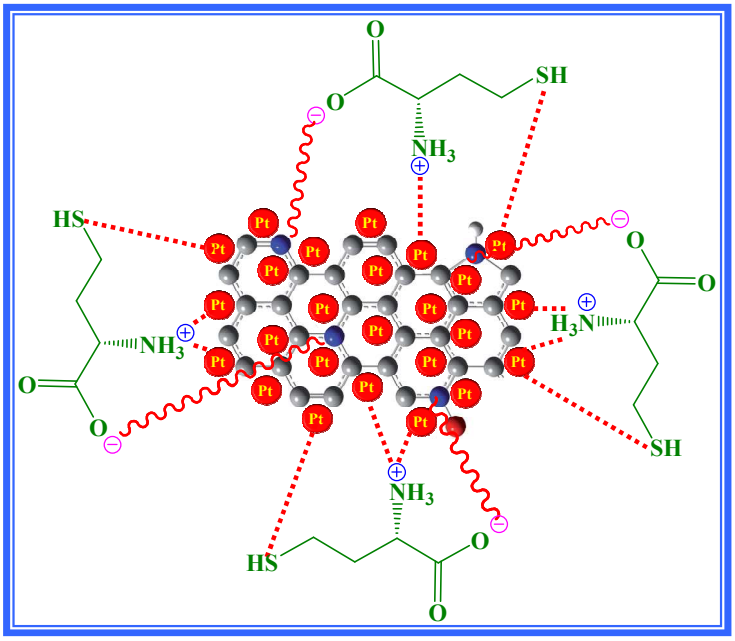

Scheme 2 Schematic representation of electrostatic and amino-Pt, thiol-Pt interactions between N-GNs/PtNPs and HCY molecule.

View Article Online
DOI: 10.1039/C3TB20923G

Graphical Abstract